Available online at www.sciencedirect.com
ScienceDirect
Trans. Nonferrous Met. Soc. China 23(2013) 1728−1736
Transactions of Nonferrous Metals Society of China
www.tnmsc.cn

Effect of heat treatment process on tensile properties of 2A97 Al−Li alloy: Experiment and BP neural network simulation

Yi LIN, Zi-qiao ZHENG, Hai-feng ZHANG, Ye HAN

School of Materials Science and Engineering, Central South University, Changsha 410083, China

Received 2 April 2012; accepted 6 September 2012

Abstract: Effects of heat treatment processes on tensile properties of 2A97 Al−Li alloy were investigated. The results show that one new heat treatment process which was developed from traditional T8 temper can effectively improve the tensile properties of Al−Li alloy. In the peak-aged condition, a large quantity of fine T_1 dispersedly precipitated in the matrix. At the same time, few secondary phases precipitated at the grain boundaries, and precipitation-free zone was unobvious. The corresponding tensile strength, yield strength and elongation of alloy were 597 MPa, 549 MPa and 7.4%, respectively. In addition, BP neural network model was developed for prediction of the tensile properties of alloy subjected to different heat treatment processes. A very good correlation between experimental and predicted results was obtained, which indicates that the BP neural network can be used for the prediction of tensile properties of 2A97 Al−Li alloy.

Key words: 2A97 Al−Li alloy; heat treatment process; tensile properties; BP neural network

1 Introduction

Al−Li alloy is one of the age-hardenable aluminum alloys. Compared with the other aluminum alloys, higher elastic modulus, lower density, higher specific strength and more favorable damage tolerance properties can be attained in Al−Li alloys. Nowadays, application of Al−Li alloys in the aerospace industry as structural components becomes an important way to reduce the mass, increase the payload and improve the fuel efficiency of aircraft [1].

The precipitation characteristics of Al−Li alloys are rather complex as the result of the affection of alloying elements. δ' (Al_3Li), θ' (Al_2Cu), S' (Al_2CuMg), T_1 (Al_2CuLi) or other phases may precipitate in the matrix during aging. The final properties of alloy products depend on their microstructures [2−7], while the microstructures are influenced by the heat treatment processes. Al−Li alloys usually undertake T8 temper which is a thermomechanical treatment including solution heat treatment, pre-deformation and artificial aging. The nucleation of θ', S' and T_1 phases is strongly promoted by pre-deformation because the application of plastic deformation prior to aging increases the density of dislocation which can act as preferable nucleation site for these phases. The pre-deformation of traditional T8 temper is generally not more than 7%. With the increase of the amount of pre-deformation, heavy precipitation of strengthening phases occurs, which enhances the strength, meanwhile may deteriorate the ductility of alloy. So developing one new heat treatment process which can enhance the strength and improve ductility of alloy is significant in exploring the potential of Al−Li alloys and extending their application in aerospace industry.

Nowadays, the artificial neural network (ANN) is one of the most powerful modelling techniques, which has been applied to modelling complicated processes in many engineering fields, such as aerospace, telecommunication, automotive and manufacturing and robotics. With ANN, a predictive model can compensate for the limitation of conventional predictive control based on the linear model and can predict the non-linear model more accurately. The basic advantage of ANN is that it is not necessary to postulate a mathematical model at first or identify its parameters. An ANN learns from data obtained from experiments and recognizes patterns in a series of input and output data sets without any prior assumptions about their interrelations. In the past few years, ANN has been developed to model different

Corresponding author: Zi-qiao ZHENG; Tel: +86-731-88830270; E-mail: s-maloy@mail.csu.edu.cn
DOI: 10.1016/S1003-6326(13)62655-2

correlations and phenomena of alloys [8−13], and provided an effective and time-saving way in developing new material and technology in different fields of materials science.

In this work, one new heat treatment was applied to improving the tensile properties of 2A97 Al−Li alloy, and the mechanism by which the heat treatment process affected the tensile properties was investigated. In addition, multi-layer artificial neural network with back-propagation (BP) learning algorithm [14] was employed to stimulate the relation between the tensile properties and the heat treatment parameters and predict corresponding tensile properties of 2A97 Al−Li alloy.

2 Experimental

The 2 mm-thick 2A97 Al−Li alloy sheets were used in this study. The samples were solution heat treated in a salt bath at 520 °C for 2 h, followed by an immediate quenching in ambient water. After quenching, these samples were divided into groups A, B and C. In the group A, samples were cold rolled to 5% reduction, and then aged at 160 °C. In the group B, samples were cold rolled to 9.5% reduction, subsequently aged at 160 °C. In the group C, samples were aged at 100 °C for 1.5 h, and then cold rolled to 5% reduction and aged at 160 °C. The heat treatment processes of 2A97 Al−Li alloy are shown in Table 1. In order to distinguish two kinds of aging, the low temperature (100 °C) aging was termed pre-aging (P.A), and the high temperature (160 °C) aging was termed secondary aging (S.A).

Table 1 Heat treatment processes of 2A97 Al−Li alloy

Process	S.T	P.D/ %	$\theta_{P.A}$/ °C	$t_{P.A}$/ h	M.D/ %	$\theta_{S.A}$/ °C	$t_{S.A}$/ h
A	520 °C for 2 h, water quenching	5	−	−	−	160	0−150
B		9.5	−	−	−	160	0−150
C		5	100	1.5	5	160	0−150

S.T−Solution treatment; P.D−Pre-deformation (cold rolling); M.D−Mid-deformation (cold rolling)

Tensile tests were performed on MTS 858 testing machine in a displacement controlled mode at a displacement rate of 2 mm/min. The tensile samples were cut from sheets along the rolling direction, and machined into bone-shape with the dimensions of 40 mm in gauge length and 10 mm in reduced section width. Three samples under different conditions were tested. An extensometer attached to the sample gauge was used to determine the strain and total elongation. The experimental errors in measurements of the stress and strain were less than 2.5%.

Microstructural features were characterized by transmission electron microscopy (TEM, Tecnai G^2 200) analysis. Slices for TEM samples were cut from tensile samples, and subsequently ground to less than 70 μm and punched into 3 mm discs. The thin foils were obtained by electrothinning at 15 V. The electrolyte was a mixture of 75% methanol and 25% nitric acid, and thinning was performed at −25 °C.

3 Establishment of BP neural network

An ANN is a mathematical model consisting of a number of highly interconnected processing neurons organized into layers, the geometry and functionality of which have been likened to that of the human brain [15]. The model has three kinds of layers of neurons: input layer, hidden layer and output layer. The neurons of the network are connected by the weights. Input layer consists of all the input factors, information from the input layer is then processed through hidden layer; following output vector is computed in the output layer. There are several algorithms in artificial neural network and one of which was used in this study was the BP training algorithm. This algorithm is one of the most famous training algorithms for multilayer perceptions, which is an iterative gradient descent technique to minimize the mean-square error (MSE) between the actual output of particular training pattern and desired output, as shown in Fig. 1.

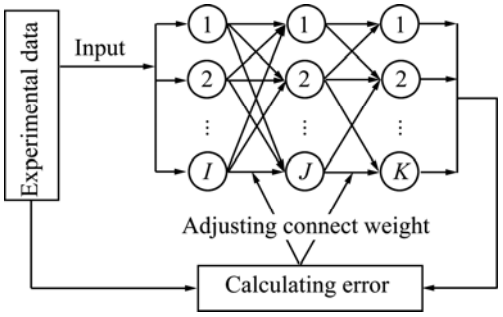

Fig. 1 Learning process and structure of ANN

In order to simulate the relationship between heat treatment parameters and tensile properties of 2A97 Al−Li alloy, a three-layer BP neural network was used. The network has five input parameters: pre-deformation, pre-aging temperature and time, mid-deformation and secondary aging time, and the output parameters of tensile strength, yield strength and elongation. So the network structure is 5-12-3, 5 corresponding to the input value, 12 to the number of hidden layer neurons and 3 to the outputs (Fig. 2).

The convergence criterion for the network is determined by MSE between the desired and predicted output values.

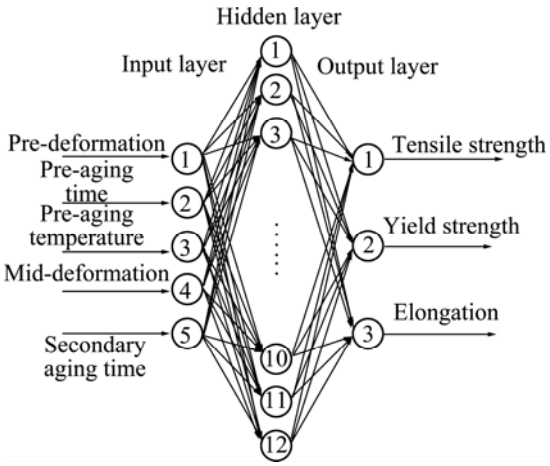

Fig. 2 Structure of three-layer BP neural network

$$\mathrm{MSE}=\frac{1}{N}\sum_{p=1}^{N}\sum_{j=1}^{3}\left(D_{pj}-O_{pj}\right)^2 \tag{1}$$

where D_{pj} and O_{pj} are the desired and predicted solution of the jth output node on the pth example, respectively, and N is the number of training samples.

BP is invoked to update all of the weights in the network according to the modified delta rule [16], which can be written as

$$\Delta W_{ij}(n+1)=\eta\delta_j H_i+\alpha\Delta W_{ij}(n) \tag{2}$$

$$\Delta V_{hi}(n+1)=\eta\delta_i A_h+\alpha\Delta V_{hi}(n) \tag{3}$$

where η is the learning rate; α is the momentum factor; V_{hi} is the weight between the input layer and hidden layer; W_{ij} is the weight between the hidden layer and the output layer; H_i is the output of the ith neural in the output layer; A_h is the input of the hth neural in the input layer; δ_j and δ_i are the error signals for neurons j and i as

$$\delta_j=(D_j-O_j)G'(\mathrm{net}_j) \tag{4}$$

$$\delta_i=\left(\sum_{j=1}^{3}W_{ij}\delta_j\right)F'(\mathrm{net}_i) \tag{5}$$

where $F(\mathrm{net}_i)$, $G(\mathrm{net}_j)$ are the transfer functions for the neurons in the hidden layer and the output layer. In this work, the hyperbolic tangent sigmoid transfer function was used for neurons in the hidden layer, and the linear transfer function was used for neurons in the output layer.

For the established BP neural network, 39 from 44 samples were randomly chosen to train the network and the remaining 5 samples were used to identify the prediction capability of the network. In this study, the BP neural network was designed, trained and tested using MATLAB package. The parameters of the network were taken as η=0.1, α=0.95 and the controlled error was 0.0001. Before training the network, both the input and output variables were normalized within the range of −1 to 1 as follows:

$$x_{\mathrm{n}}=2\frac{x-x_{\min}}{x_{\max}-x}-1 \tag{6}$$

where x_{n} is the normalized value of x, and $x_{\min}$ and $x_{\max}$ are the minimum and maximum values of x.

4 Results and discussion

4.1 Tensile properties

The aging curves of alloy subjected to different heat treatment processes are shown in Fig. 3. It can be seen

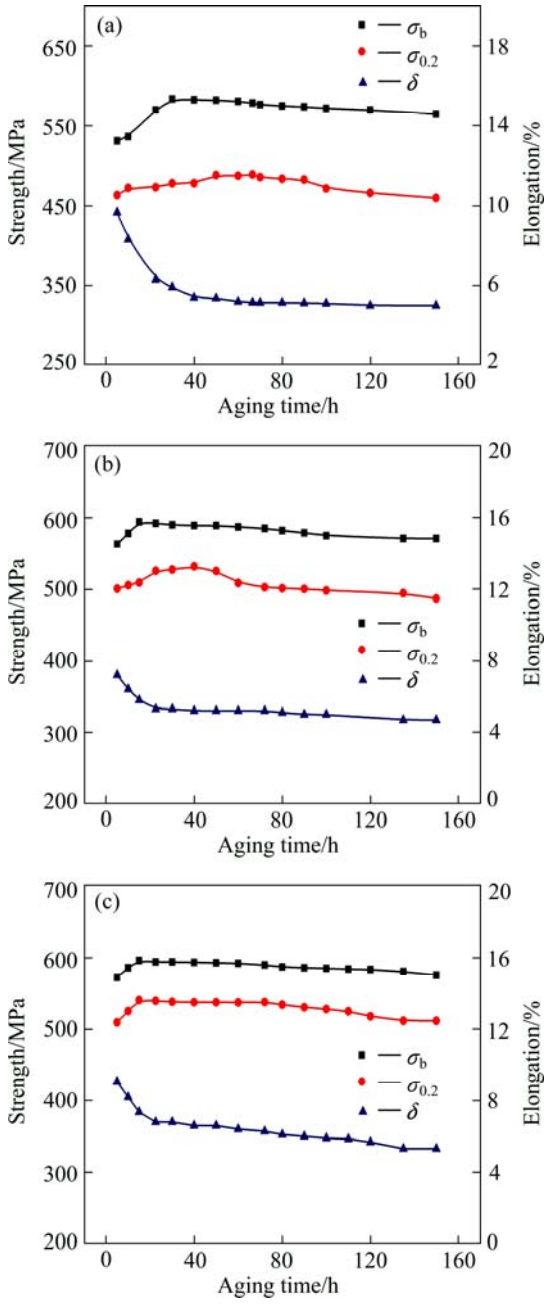

Fig. 3 Relationship between tensile properties and aging time of 2A97 Al−Li alloy by heat treatment processes A (a), B (b) and C (c)

that peak aging is achieved after aging at 160 °C for 30 h by process A. The tensile strength, yield strength and elongation are 584 MPa, 478 MPa and 6.0%, respectively. By process B, the peak aging is obtained after aging at 160 °C for 16 h. The tensile strength, yield strength and elongation are 592 MPa, 508 MPa and 5.8%, respectively. In the condition of process C, the peak aging is reached after the secondary aging at 160 °C for 16 h. The tensile strength, yield strength and elongation are 597 MPa, 549 MPa and 7.4%, respectively. Compared with process A, processes B and C can effectively improve the strength, and shorten the response time of aging. However, the ductility of alloy which is subjected to process B is undesirable. The total amount of deformation of process C is equal to that of process B, but the alloy, which suffers smaller deformation, twice by process C, obtained more favorable tensile properties in the peak-aged condition. The peak-aged tensile properties of alloy which was subjected to different heat treatment processes are shown in Table 2.

Table 2 Peak-aged tensile properties of 2A97 Al−Li alloy subjected to different heat treatment processes

Process	σ_b/MPa	$\sigma_{0.2}$/MPa	δ/%
A	584	478	6.0
B	592	508	5.8
C	597	549	7.4

4.2 Microstructure

Figure 4 shows the TEM images and corresponding SAED patterns of 2A97 Al−Li alloy in different peak-aged conditions, viewed along $\langle 112 \rangle_\alpha$ direction. It can be seen that plate-shaped T_1 phases precipitate in the matrix of alloy. In the peak-aged condition, coarse T_1 phases distribute widely in the matrix of alloy subjected to process A (Fig. 4(a)). The alloy which undertaken process B obtains fine and dispersed T_1 phases (Fig. 4(b)). By process C, more high density of fine T_1 phases and a small number of S' phases are obtained in the peak-aged condition (Fig. 4(c)). Above observation of microstructure indicates that pre-deformation and mid-deformation can effectively promote the nucleation of T_1 phase and alter its precipitation characteristic.

Generally, dislocations can promote the precipitation of T_1 phases. With increase of the amount of deformation, more dislocation will be introduced to the matrix, so more T_1 phases are obtained in alloys by process B or C. Process C applied intense deformation to the alloy by twice smaller deformation, namely pre-deformation and mid-deformation. The twice smaller deformation was interrupted by a low temperature aging which ensured the uniform deformation of alloy and introduced uniform distribution dislocations to the matrix. In that case, the alloy obtained higher density of fine T_1 phases and a highest strength after secondary aging at 160 °C for 16 h.

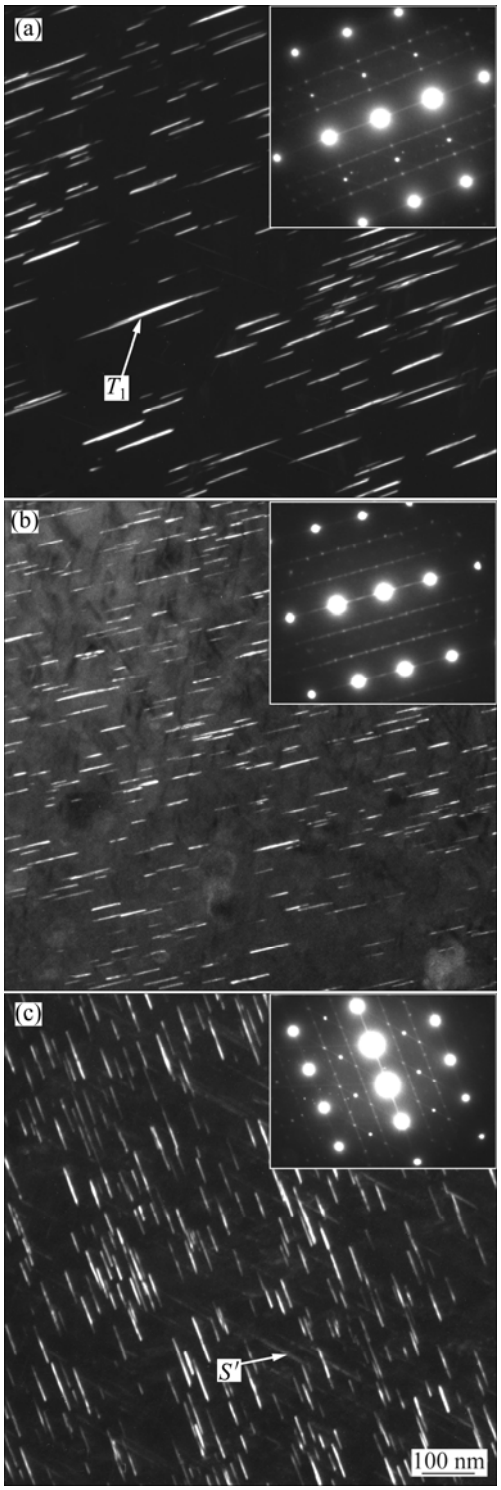

Fig. 4 TEM images of peak-aged 2A97 Al−Li alloy subjected to processes A (a), B(b) and C(c), and corresponding SAED patterns along $\langle 112 \rangle_\alpha$

Figure 5 shows the microstructure of grain

boundaries in different peak-aged conditions. Secondary phases and precipitate-free zone (PFZ) were observed at the grain boundaries of alloy subjected to processes A and B, as shown in Figs. 5(a) and (b). By process C, grain boundary phases and PFZ could not be observed (Fig. 5(c)).

During aging process, T_1 and δ(AlLi) phases usually nucleated and grew at grain boundaries that induced solution depletion near grain boundaries resulting in formation of PFZ. The alloy which was subjected to process C obtained more uniform T_1 phases within the grains. Heavy precipitation of T_1 phases consumed lots of solute atoms that reduced the quantities of grain boundary phases, so the secondary phases and PFZ were unobvious at grain boundaries. However, there were secondary phases and PFZ at the grain boundaries of alloy, which was subjected to process B. It is due to the fact that large deformation applied to alloy at one time did not promote the uniform precipitation of T_1 phases in the grains.

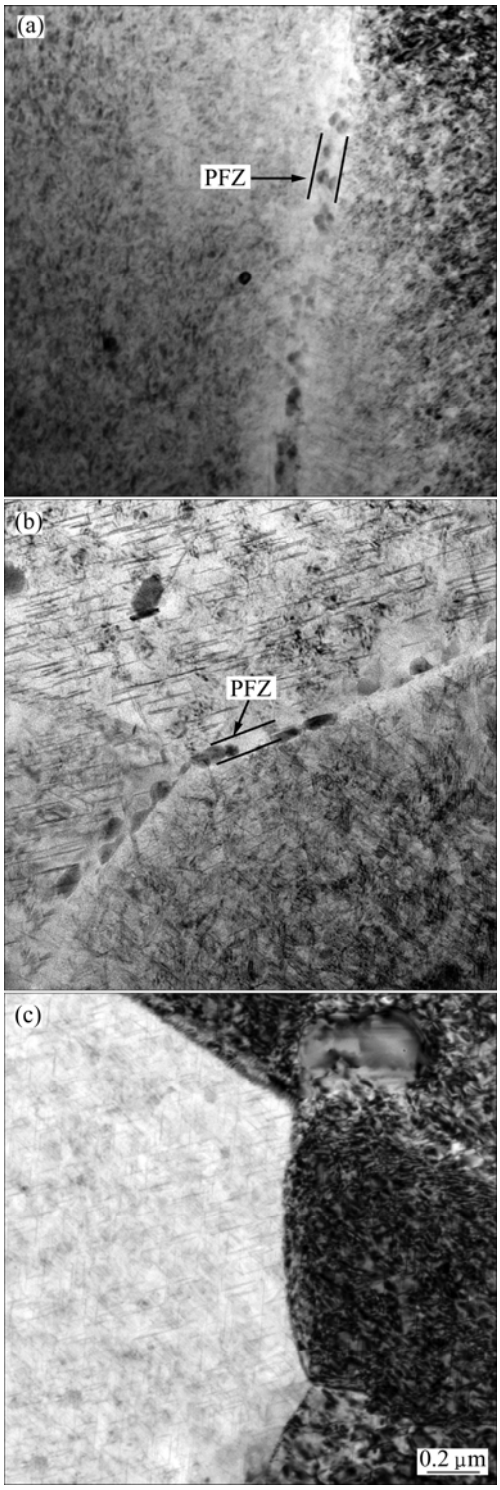

Fig. 5 Microstructures of grain boundaries of peak-aged 2A97 Al−Li alloy subjected to processes A (a), B(b) and C(c)

The PFZ is soft with respective to interior of grain containing precipitates, and the flow stress in PFZ is lower than that in the region within the grain, so PFZ will deform more easily than the interior of grain [17]. The deformation takes place preferentially in the soft PFZ, leading to stress concentration of grain boundaries. The high stress concentration at the grain boundaries and at grain boundary triple junctions promotes propagation and coarsening of cracks, resulting in low energy intergranular fracture of alloy. Therefore, the alloy which is subjected to process C obtains more preferable ductility in the peak-aged condition.

It is interesting that the alloy obtained a few of S' phases in the peak-aged condition by process C, but the mechanism by which S' phases precipitated will not be discussed in this work. The S' phases have open-packed structure, and there are no uniform densely packed potential slip planes within the S' phases which lie parallel to the matrix slip planes. Therefore, the S' phases prevent the development of bands of coplanar slip and promote uniform deformation [18]. Therefore, process C improves the peak-aged ductility of alloy by the dispersing slip of S' phases to some extent.

4.3 Simulation

During the training procedure, the MSE decreased with increasing number of iteration. The performance changing of network in training stage is shown in Fig. 6.

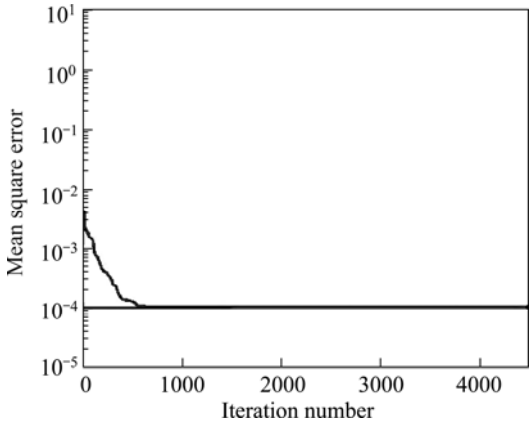

Fig. 6 Performance changing of BP neural network at training stage

It can be seen that the significant influence on error reduction is not changed after 4476 training cycles. After being trained, the BP neural network model can map the non-linear relationship between tensile properties and heat treatment parameters. Comparison between experimental and BP neural network predicted tensile properties of 2A97 Al−Li alloy in different heat treatment processes at training stage is shown in Fig. 7. It can be clearly seen that the BP neural network is properly trained and shows a consistency among the tensile properties. Regression analysis between the experimental and predicted tensile properties at training stage is shown in Fig. 8. Figure 8 shows that the slop and intercept of the regression equations for the prediction are significantly near to 1 and 0, and it is difficult to distinguish the best fit line from perfect fit line (predicted data are equal to experimental data). This indicates that the BP neural network has a perfect fit between experimental and predicted tensile properties at training

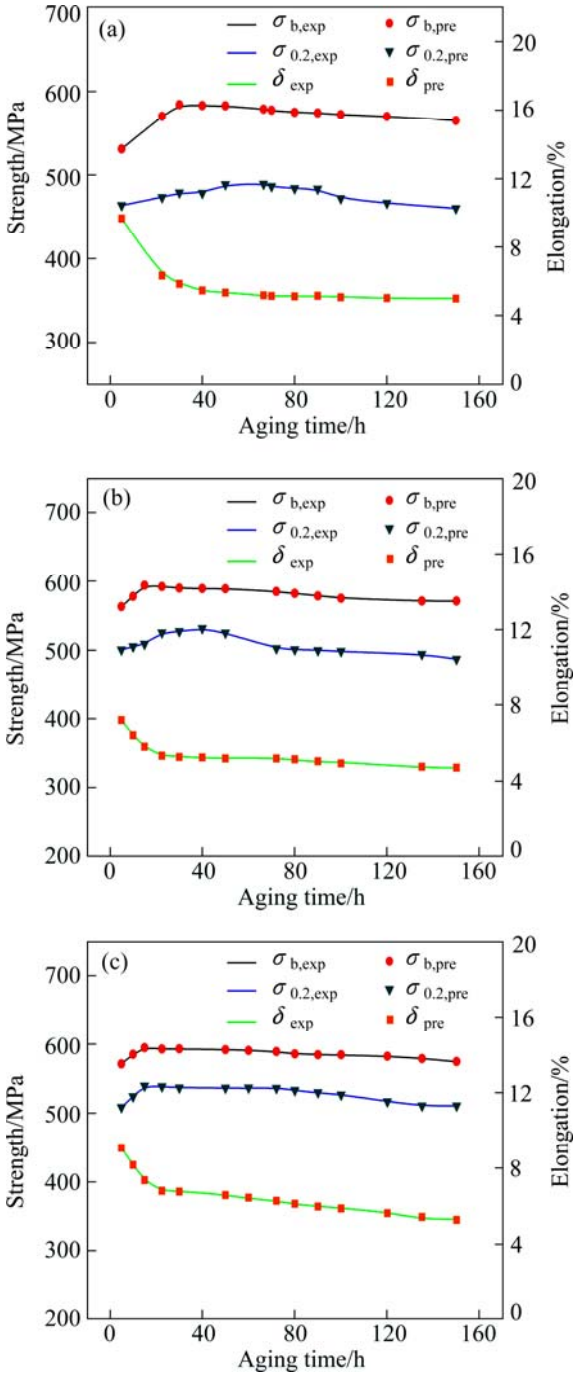

Fig. 7 Comparison between experimental and predicted tensile properties of 2A97 Al−Li alloy subjected to heat treatment processes A (a), B (b) and C (c) for training data sets

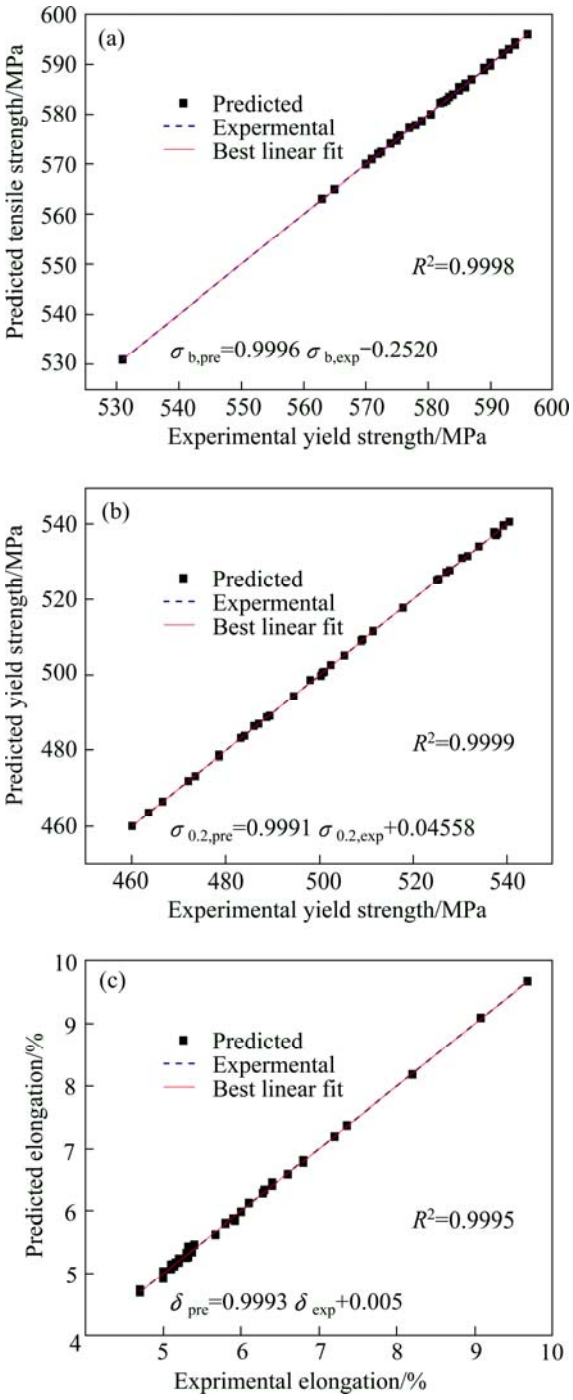

Fig. 8 Regression analysis between experimental and predicted tensile strength (a), yield strength (b) and elongation (c) of 2A97 Al−Li alloy for training data sets

stage. For the purpose of identifying the prediction performance with regards to the testing data, a comparison of the experimental and predicted tensile properties of 2A97 Al−Li alloy for 5 testing data sets which have never been seen by the network has been conducted, as shown in Fig. 9. Comparison of experimental and predicted tensile properties at testing stage indicates that there is a high correlation between them. Regression analyses between the experimental and predicted tensile properties are shown in Fig. 10. It can be seen that the slop and intercept of the regression equations for the prediction are close to 1 and 0 respectively, and the relation coefficients (R) are almost 1, so the predicted results can accurately reflect the corresponding tensile properties of alloy. Additionally, the performance accuracy was reproved by statistical analysis of the relative error between prediction and experiment (Fig. 11). It can be observed that there is a less variation between predicted and experimental values; the relative errors are all within 2.5%. It should be noted that the relative errors of tensile strength and yield strength are smaller than those of elongation because the experimental strengths are very large.

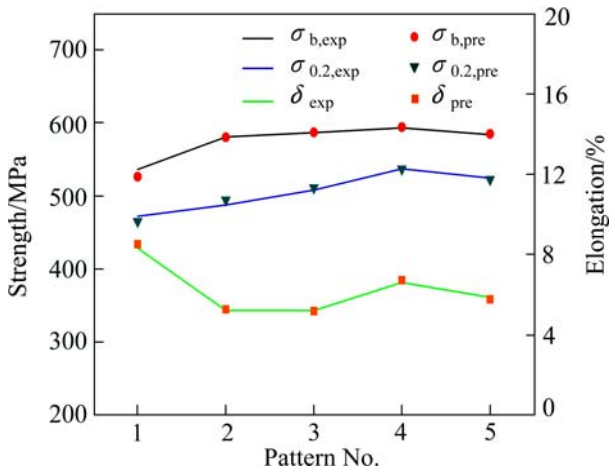

Fig. 9 Comparison between experimental and predicted tensile properties of 2A97 Al−Li alloy for testing data sets

The BP neural network used in this work provided the weights listed in Tables 3 and 4. The neural net weight matrix can be used to assess the relative importance of the various heat treatment parameters on the tensile properties. Connection weights were partitioned by the method which was proposed first by GARSON [19]. The relative importance of various heat treatment parameters is shown in Table 5. It can be seen that all of the heat treatment parameters have strong effects on the tensile properties of 2A97 Al−Li alloy. The secondary aging appears to be the most influential parameter. However, a relative importance of 37.79% of

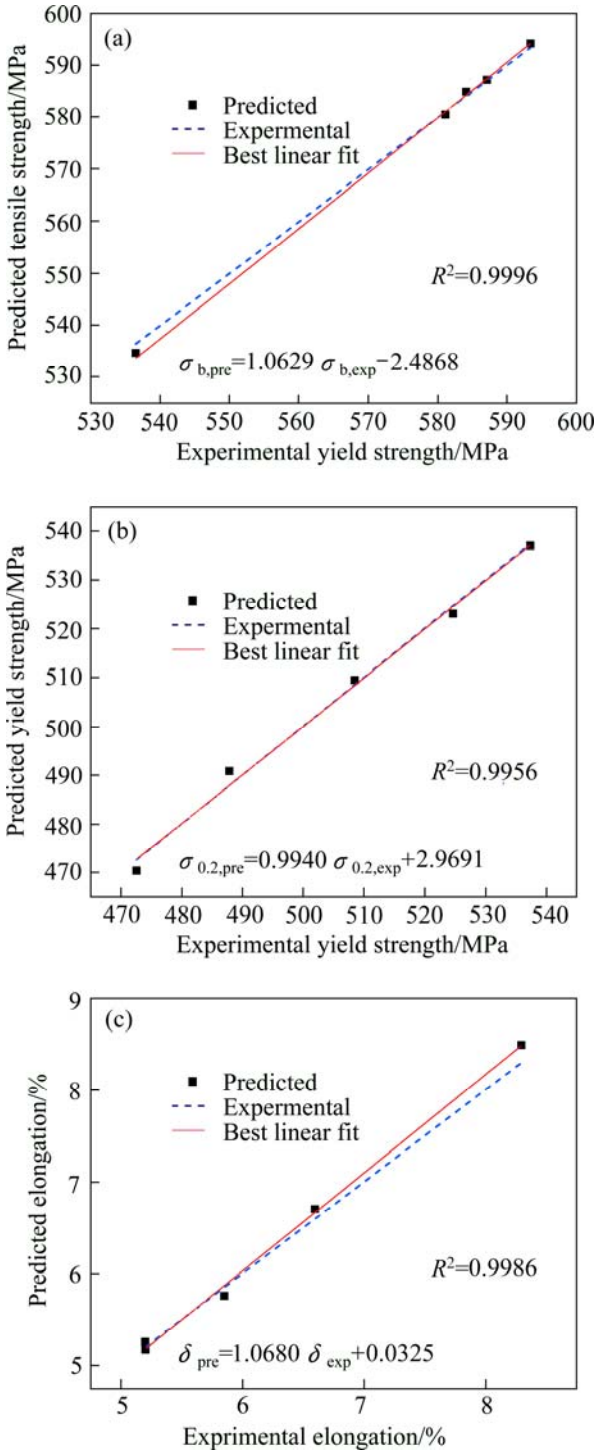

Fig. 10 Regression analysis between experimental and predicted tensile strength (a), yield strength (b) and elongation (c) of 2A97 Al−Li alloy for testing data sets

combination influent of pre-aging and mid-deformation shows that the combination of pre-aging and mid-deformation plays an important role in affecting the tensile properties of 2A97 Al−Li alloy. Further, traditional T8 temper combining with pre-aging and mid-deformation may become an effective process in extending the potential of Al−Li alloy.

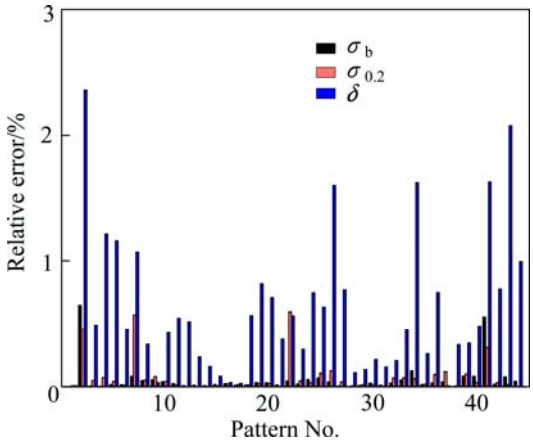

Fig. 11 Relative errors between experimental and predicted tensile properties of 2A97 Al−Li alloy for all data sets

Table 3 Weights between input and hidden layers

Neuron No.	P.D	$\theta_{P.A}$	$t_{P.A}$	M.D	$t_{S.A}$
1	3.7688	−1.4841	−1.5503	−1.0813	4.6693
2	−0.2861	1.4341	−0.8694	0.5974	−2.2194
3	−0.7200	1.5036	−0.3295	−0.5808	5.1984
4	0.7311	−0.6074	−0.1604	−0.8512	−0.4586
5	−4.5496	0.2792	−1.8247	−0.1062	−3.9837
6	1.4247	−2.4773	−0.2145	−0.8621	−2.4967
7	−4.1570	−0.9919	−0.1400	−0.4855	−3.8689
8	−4.0599	−3.9800	−1.4571	−2.3261	−13.4445
9	2.1699	3.9324	3.8063	2.6220	−8.2745
10	−1.0156	6.9057	7.8919	5.8373	20.6115
11	−0.3955	−1.1754	−1.5005	−0.6949	3.1196
12	−0.7562	0.5142	−0.2083	−1.9142	−11.9132

Table 4 Weights between hidden and output layers

Neuron No.	σ_b	$\sigma_{0.2}$	δ
1	−0.0586	1.4627	0.1972
2	0.3441	0.1587	0.2016
3	−0.5014	0.5504	−2.0682
4	1.4983	−3.9623	−0.5586
5	1.9293	−1.2166	6.8306
6	−0.5432	2.5099	0.1983
7	−1.9296	1.4979	−6.8330
8	0.0125	0.3304	0.0294
9	0.4410	−0.5313	−0.0766
10	0.2687	0.6309	−0.1070
11	−0.1657	−0.1259	−0.2335
12	−1.2692	0.3513	−0.6471

Table 5 Relative importance of input variables on tensile properties of 2A97 Al−Li alloy (%)

P.D	$\theta_{P.A}$	$t_{P.A}$	M.D	$t_{S.A}$
17.84	16.29	10.44	11.06	44.37

5 Conclusions

1) One new heat treatment process consisting of solution treatment, pre-deformation, pre-aging, mid-deformation, and secondary aging is developed. And 2A97 Al−Li alloy obtains favorable tensile properties by this new heat treatment. In the peak-aged condition, the tensile strength, yield strength and elongation of alloy are 597 MPa, 549 MPa and 7.4%, respectively. At this stage, a large number of T_1 phases precipitate in the matrix, and few secondary phases are observed at the grain boundaries.

2) The BP neural network reflecting the inherent law between the experimental data is built with heat treatment parameters and tensile properties. According to the selected process parameters of heat treatment, the BP neural network can accurately foresee the tensile properties of 2A97 Al−Li alloy. The predicted results show that the secondary aging appears to be the most influential parameter on tensile properties of 2A97 Al−Li alloy, and the combination of pre-aging and mid-deformation also plays an importance role in improving the tensile properties of the alloy.

References

[1] RIOJA R J,LIU J. The evolution of Al−Li base products for aerospace and space applications [J]. Metallurgical and Materials Transactions A, 2012, 43(9): 3325−3337.

[2] NOBLE B, THOMPSON G. Precipitation characteristics of aluminium−lithium alloys [J]. Metal Science, 1971, 5(1): 114−120.

[3] GREGSON P J, FLOWER H M. Microstructural control of toughness in aluminium-lithium alloys [J]. Acta Metallurgica, 1985, 33(3): 527−537.

[4] LI J F, ZIQIAO Z, NA J, CHENGYU T. Localized corrosion mechanism of 2××× series Al alloy containing S(Al_2CuMg) and θ′(Al_2Cu) precipitates in 4.0% NaCl solution at pH 6.1 [J]. Materials Chemistry and Physics, 2005, 91(2−3): 325−329.

[5] KIM H J, NIINOMI M. The role of microstructures on the strengthening mechanisms of a thermomechanically processed 2091 Al−Li alloy [J]. Materials Science and Engineering A, 2000, 284(1−2): 14−24.

[6] HUANG J, ARDELL A. Crystal structure and stability of T_1 precipitates in aged Al−Li−Cu alloys [J]. Materials Science and Technology, 1987, 3(3): 176−188.

[7] LAVERNIA E J, SRIVATSAN T S, MOHAMED F A. Strength, deformation, fracture behaviour and ductility of aluminium-lithium alloys [J]. Journal of Materials Science, 1990, 25(2): 1137−1158.

[8] GUPTA A K, SINGH S K, REDDY S, HARIHARAN G. Prediction of flow stress in dynamic strain aging regime of austenitic stainless steel 316 using artificial neural network [J]. Materials & Design, 2012, 35: 589−595.

[9] SUN Y, ZENG W D, HAN Y F, MA X, ZHAO Y Q. Optimization of chemical composition for TC11 titanium alloy based on artificial neural network and genetic algorithm [J]. Computational Materials Science, 2011, 50(3): 1064−1069.

[10] MEHMET SIRAC O. Artificial neural network approach to predict the electrical conductivity and density of Ag−Ni binary alloys [J]. Journal of Materials Processing Technology, 2008, 208(1−3): 470−476.
[11] SHABANI M, MAZAHERY A. Modeling of the wear behavior in A356−B_4C composites [J]. Journal of Materials Science, 2011, 46(20): 6700−6708.
[12] ALTINKOK N, KOKER R. Use of artificial neural network for prediction of physical properties and tensile strengths in particle reinforced alüminum matrix composites [J]. Journal of Materials Science, 2005, 40(7): 1767−1770.
[13] LAKSHMINARAYANAN A, BALASUBRAMANIAN V. Comparison of RSM with ANN in predicting tensile strength of friction stir welded AA7039 aluminium alloy joints [J]. Transactions of Nonferrous Metals Society of China, 2009, 19(1): 9−18.
[14] BASHEER I A, HAJMEER M. Artificial neural networks: fundamentals, computing, design, and application [J]. Journal of Microbiological Methods, 2000, 43(1): 3−31.
[15] JAIN A K, MAO J, MOHIUDDIN K M. Artificial neural networks: A tutorial [J]. Computer, 1996, 29(3): 31−44.
[16] GASTEIGER J, ZUPAN J. Neural networks in chemistry [J]. Angewandte Chemie International Edition in English, 1993, 32(4): 503−527.
[17] KAWABATA T, IZUMI O. Ductile fracture in the interior of precipitate free zone in an Al−6.0%Zn−2.6%Mg alloy [J]. Acta Metallurgica, 1976, 24(9): 817−825.
[18] FLOWER H M, GREGSON P J. Solid state phase transformations in aluminium alloys containing lithium [J]. Materials Science and Technology, 1987, 3(2): 81−90.
[19] GARSON G D. Interpreting neural-network connection weights [J]. AI Expert, 1991, 6(4): 46−51.

热处理工艺对 2A97 Al–Li 合金拉伸性能的影响：实验和 BP 人工神经网络模拟

林 毅，郑子樵，张海锋，韩 烨

中南大学 材料科学与工程学院，长沙 410083

摘 要：研究热处理工艺对 2A97 Al−Li 合金拉伸性能的影响。结果表明：从传统 T8 工艺改进的、具有预时效和中间变形的热处理工艺可以有效地改进 Al−Li 合金的拉伸性能。合金经该热处理工艺处理后，在峰时效条件下，基体中析出大量的 T_1 相，同时，晶界无第二相析出，并且晶界上无沉淀析出带不明显。峰时效合金的抗拉强度、屈服强度和伸长率分别为 597 MPa、549 MPa 和 7.4%。此外，建立 BP 人工神经网络模型对经不同热处理工艺处理的合金的拉伸性能进行预测，所得预测结果与实验结果吻合较好，表明该人工神经网络模型可用于预测 2A97 Al−Li 合金的拉伸性能。

关键词：2A97 AL−Li 合金；热处理工艺；拉伸性能；BP 人工神经网络

(Edited by Xiang-qun LI)